Frontiers in Computing and Intelligent Systems
ISSN: 2832-6024 | Vol. 11, No. 1, 2025

Simulation Analysis of Powered Parachute Motion Characteristics based on Motor Thrust and Flap Deflection Control

Bailin Zhu, Yan Shi *

School of traffic & transportation, Chongqing Jiaotong University, Chongqing, 400074, China
* **Corresponding author**: Yan Shi (Email: 622220950134@mails.cqjtu.edu.cn)

Abstract: In this paper, a distributed new type of parafoil is proposed, conducting its dynamic modeling and motion characteristic analysis, thereby laying the foundation for subsequent trajectory tracking research and physical experimentation. First, the dynamics of the parafoil and payload are analyzed, and the dynamic model of the entire parafoil system is derived from this analysis. Then, the kinematic characteristics under control inputs of bilateral pull-down, unilateral pull-down, and unilateral pull-down with differential thrust are examined using the simulation model; Simulation results indicate that the established 8-DOF dynamic model accurately describes the parafoil's motion. The proposed differential control increases yaw motion response speed and provides a basis for subsequent trajectory tracking research and physical experiments. The proposed differential control enhances the yaw motion response speed and reduces the relative motion between the wing parachute and payload to a certain extent. Simulation analysis verifies the model's validity and the control method's feasibility.

Keywords: Distributed Layout; Dynamic Modelling; Simulation System; Characterisation.

1. Introduction

Unmanned Aerial Vehicles (UAVs) are experiencing burgeoning utilization within the transportation sector [1]. Rotary-wing UAVs are predominantly favored owing to their versatile functionality, enabling vertical take-off, landing, and hovering through propeller rotation for lift. However, they suffer from high energy consumption, limited endurance, and payload capacity. Conversely, fixed-wing UAVs generate lift via their wing structures, offering rapid flight speeds suitable for long-distance cruising, yet they necessitate extended runways for take-off and landing and are incapable of hovering [2]. Consequently, there is a pressing demand for an innovative transportation vehicle characterized by substantial payload capacity, extended endurance, and superior applicability within the transportation domain.

The powered parafoil represents a novel category of flexible wing vehicles [3]. The powered parafoil comprises a wing parachute and a payload. During flight, the parachute's air chamber inflates to provide lift [4], while engine thrust is employed solely for attitude or positional adjustments. This configuration ensures long endurance and stable flight under substantial payloads, characterized by minimal take-off and landing requirements, exceptional low-speed performance, and structural simplicity [5]. Leveraging unmanned aircraft technology and artificial intelligence, intelligent autonomous unmanned powered parafoils have been developed, significantly enhancing their autonomous flight capabilities and mission execution efficiency. Given these advancements, the powered parafoil demonstrates significant advantages across various application scenarios, including cargo transport, agricultural and forestry protection, environmental monitoring, and rescue missions.

The 6 Degrees of Freedom (DOF) model [6-7] considers the wing parachute and payload as rigidly connected, thus precluding any relative motion. The 8 DOF model [8] incorporates relative motions in the pitch and yaw directions, building upon the 6 DOF model, thereby facilitating the analysis of relative motion states between the wing parachute and payload. Chen [9] utilized the longitudinal model to fit the relationship between motor rotational speed and propeller thrust, thereby enhancing longitudinal control efficacy. Li [10] accounted for external wind fields and various complex disturbances, establishing a dynamic model for the DOF parafoil system under such conditions. Zhu [11] simulated and analyzed the fundamental kinematic characteristics and responses to wind and thrust using the 8 DOF dynamics model based on Kirchhoff's equations of motion. Li [12] examined the impact of additional mass on the kinematic model, providing calculations for this additional mass, and analyzed the effects of flap deflection on the aerodynamic forces and moments of the wing parachute.

Despite significant advancements in parafoil research, there remain notable deficiencies in control accuracy, response speed, and payload capacity. These issues are particularly pronounced in complex environments, where control of the parafoil is markedly inadequate. To address these challenges, this paper proposes a novel distributed differential control parafoil, as illustrated in Fig. 1. Two motors are positioned on either side of the payload's tail to provide thrust, enabling differential thrust to enhance payload capacity, control accuracy, and response speed of the powered parafoil, thereby advancing the development and application of unmanned powered parafoils.

The structure of this paper is as follows: Section 2 establishes the coordinate system and defines the kinematic equations of the parafoil. Section 3 develops an eight DOF dynamics model for the distributed parafoil. Section 4 presents simulation experiments to verify the model's validity and characterize its performance. Finally, the paper summarizes the research findings and outlines future research directions.

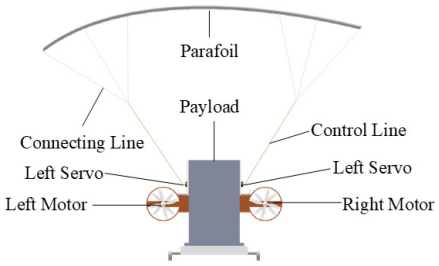

Fig 1. Structure of the distributed parafoil

2. Coordinate System and Equations of Motion

Modeling the 8 DOF dynamics of a powered parachute necessitates three coordinate systems: the geodetic coordinate system, the wing parachute coordinate system, and the load coordinate system. All these coordinate systems conform to the right-handed coordinate system, as depicted in Fig. 2.

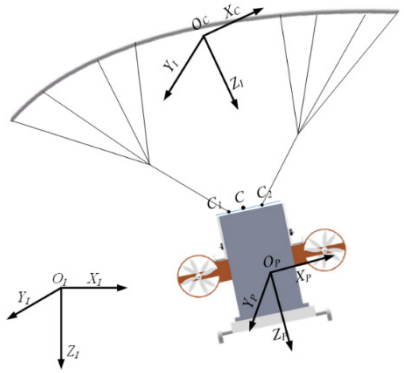

Fig 2. Schematic diagram of coordinate system

Define the geodetic coordinate system as an inertial coordinate system, denoted as $O_ix_iy_iz_i$, with the x-axis pointing to the direction of parachute motion, the y-axis pointing to the right, and the z-axis vertically downward and perpendicular to the x-axis; define the wing parachute coordinate system, denoted as $O_cx_cy_cz_c$, with the center of mass of the parachute O_c as the origin, with the x-axis pointing to the direction of the wing parachute motion, the y-axis pointing to the right, and the z-axis vertically downward and perpendicular to the x-axis; and define the payload coordinate system Define the load coordinate system, denoted as $O_px_py_pz_p$, with the load center of mass O_P as the origin, x-axis pointing to the direction of payload movement, y-axis pointing to the right, z-axis vertically downward and perpendicular to the x-axis. The Euler angles of the wing parachute coordinate system $O_cx_cy_cz_c$ and the origin of the load coordinate system $O_px_py_pz_p$, in the inertial coordinate system $O_ix_iy_iz_i$ are denoted as $(\varphi_c,\theta_c,\psi_c)$ and $(\varphi_p,\theta_p,\psi_p)$, respectively.

The transformation matrix between the geodetic coordinate system and the wing parachute coordinate system is defined by three Euler angles $(\varphi_c,\theta_c,\psi_c)$, with the transformation relationship given as follows:

$$T_{IC}=\begin{bmatrix} \mathrm{c}\theta\mathrm{c}\psi & \mathrm{c}\theta\mathrm{s}\psi & -\mathrm{s}\theta \\ \mathrm{s}\phi\mathrm{s}\theta\mathrm{c}\psi-\mathrm{c}\phi\mathrm{s}\psi & \mathrm{s}\phi\mathrm{s}\theta\mathrm{s}\psi+\mathrm{c}\phi\mathrm{c}\psi & \mathrm{s}\phi\mathrm{c}\theta \\ \mathrm{s}\phi\mathrm{s}\theta\mathrm{c}\psi+\mathrm{s}\phi\mathrm{s}\psi & \mathrm{c}\phi\mathrm{s}\theta\mathrm{s}\psi-\mathrm{s}\phi\mathrm{c}\psi & \mathrm{c}\phi\mathrm{s}\theta \end{bmatrix} \tag{1}$$

where for any angle α has $\alpha=\alpha_c$, $sin\alpha=s\alpha$ and $cos\alpha=c\alpha$.

$$\begin{bmatrix} \dot{x} \\ \dot{y} \\ \dot{z} \end{bmatrix} = T_{I-C}^{T}\begin{bmatrix} u \\ v \\ w \end{bmatrix} \tag{2}$$

where x, y, and z are the position components of the power parachute in the geodetic coordinate system, and u, v, and w are the velocity components in the wing parachute coordinate system.

$$\begin{bmatrix} \dot{\phi} \\ \dot{\theta} \\ \dot{\psi} \end{bmatrix} = \begin{bmatrix} 1 & \mathrm{s}\phi\,\mathrm{t}\theta & \mathrm{s}\phi t\theta \\ 0 & \mathrm{c}\phi & -\mathrm{s}\phi \\ 0 & \mathrm{s}\phi/\mathrm{c}\theta & \mathrm{c}\phi/\mathrm{c}\theta \end{bmatrix}\begin{bmatrix} p \\ q \\ r \end{bmatrix} \tag{3}$$

where for any angle α has $\alpha=\alpha_c$, $tan\alpha=t\alpha$, and φ, θ, ψ denote roll, pitch, and yaw angles, respectively, and q, p, r denote angular velocity components in the wing parachute coordinate system, respectively.

The relative transverse roll motion between the wing parachute and the payload is negligible. The transformation matrix from the wing parachute coordinate system to the payload coordinate system is defined by the relative pitch angle θ_{pc} and the relative yaw angle ψ_{pc}, with the transformation matrix given as follows:

$$T_{pc}=\begin{bmatrix} c\theta_{pc}c\psi_{pc} & -s\psi_{pc} & s\theta_{pc}c\psi_{pc} \\ c\theta_{pc}s\psi_{pc} & c\psi_{pc} & s\theta_{pc}s\psi_{pc} \\ -s\theta_{pc} & 0 & c\theta_{pc} \end{bmatrix} \tag{4}$$

3. Dynamic Modelling of Parafoils

To render the powered parachute system analyzable, the modeling process necessitates the following assumptions:

(1) The fully inflated wing parachute exhibits longitudinal symmetry, and its aerodynamic shape remains constant;

(2) The center of mass of the wing parachute coincides with its aerodynamic center of pressure and, although not overlapping with the center of gravity, lies on the same longitudinal axis;

(3) The payload is considered a regularly shaped rectangle, with its lift neglected and only its aerodynamic drag accounted for;

(4) The ground is assumed to be planar, implying that the gravitational acceleration of the Earth is constant.

3.1. Coordinate System and Equations of Motion

The forces and their moments on the wing parachute are aerodynamic force F_{cA} and its moment M_{cA}, gravitational force F_{cG}, inertial force F_{cI} and its moment M_{cI}, and connecting line tension F_{cT} and its moment M_{cT}, so the equation of state of the wing parachute with respect to the forces and their moments is as follows:

$$\begin{aligned} E_{Fc}\dot{x} &= -\left(F_{cG}+F_{cAR}+F_{cAB}+F_{cT}\right) \\ E_{Mc}\dot{x} &= -\left(M_{cAR}+M_{cAB}+M_{cT}+M_{cI1}\right) \end{aligned} \tag{5}$$

where

$$E_{Fc}=\left[\left(m_cI_3+M_a\right)\quad 0_{3\times 9}\right]^T \tag{6}$$

$$E_{Mc}=\left[0_{3\times 3}\quad J_a+J_c\quad 0_{3\times 6}\right]^T \tag{7}$$

$$x=\left[V_c^T\quad \omega_c{}^T\quad \omega_{pc}{}^T\quad \theta_{pc}\quad \psi_{pc}\quad \phi_c\quad \theta_c\right]^T \tag{8}$$

$$F_{cG}=m_cg\left[-\mathrm{s}\theta_c\quad \mathrm{c}\theta_c\mathrm{s}\phi_c\quad \mathrm{c}\theta_c\mathrm{c}\phi_c\right]^T \tag{9}$$

$$F_{cAR}=\sum_{i=1}^{8}B_{i-O_c}\left(F_{Li}+F_{Di}\right) \tag{10}$$

$$M_{cAR}=\sum_{i=1}^{8}L^{\times}{}_{O_c-i}B_{i-O_c}\left(F_{Li}+F_{Di}\right) \tag{11}$$

$$F_{cAB}=0.5\rho V_c^2S_cC_{BL}\delta_e\begin{bmatrix}\sin\alpha_c\\0\\-\cos\alpha_c\end{bmatrix}+0.5\rho V_c^2S_cC_{BY}\delta_a\begin{bmatrix}0\\1\\0\end{bmatrix}$$
$$+0.5\rho V_c^2S_cC_{BD}\delta_e\begin{bmatrix}-\cos\alpha_c\cos\beta_c\\-\sin\beta_c\\-\sin\alpha_c\cos\beta_c\end{bmatrix} \tag{12}$$

$$M_{cAB}=0.5\rho V_c^2S_c\left\{\begin{matrix}b_c\delta_e\left[0\quad C_{M\delta}\quad 0\right]^T\\+c_c\delta_a\left[C_{R\delta}\quad 0\quad C_{N\delta}\right]^T\end{matrix}\right\} \tag{13}$$

In particular, when calculating the aerodynamic forces and moments generated by the wing parachute and the internal gas, the wing parachute is divided into eight equal segments along the spreading direction [13], and then the aerodynamic forces and moments of each segment are calculated, and the total aerodynamic forces of the wing parachute can be obtained by cumulatively summing up the aerodynamic forces as shown in Fig. 3. The equations for lift and drag can be expressed as follows:

$$F_{Li}=k_iC_{Li}\left(0.5\rho S_{ci}\sqrt{u^2{}_{ci}+w^2{}_{ci}}\right)\left[w_{ci}\quad 0\quad -u_{ci}\right]^T \tag{14}$$

$$F_{Di}=-C_{Di}\left(0.5\rho S_{ci}\sqrt{V^2{}_{ci}}\right)\left[u_{ci}\quad v_{ci}\quad w_{ci}\right] \tag{15}$$

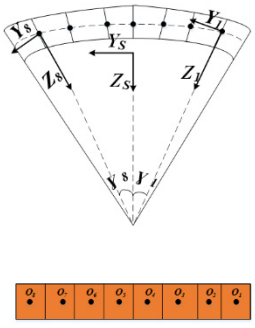

Fig 3. Schematic diagram of wing parachute segmentation

where, the subscript c represents the wing parachute; m_c denotes the wing parachute mass; I_3 denotes the third-order unit matrix; $\mathbf{0}_{m\times n}$ denotes the **0** matrix with m rows and n columns; Ma is the additional mass matrix; Ja is the additional mass inertia matrix; J_c is the wing parachute rotational inertia matrix; g denotes the gravitational acceleration; ρ denotes the atmospheric density; S_c denotes the wing parachute area; the subscripts L, D denote the lift and the drag force, respectively; k_i denotes the product factor, whose values in each segment are 0.6, 1.0, 1.16, and 1.24 from inside to outside, respectively; C_{Li} and C_{Di} denote the lift and drag coefficients, respectively; ρ denotes the atmospheric density; S_{Ci} denotes the area of each segment; $V_{ci}=[u_{ci}\ v_{ci}\ w_{ci}]^T$, which denotes the velocity of each segment of the wing parachute, and u_{ci}, v_{ci} ,and w_{ci} denote the components of the velocity; and $B_{i\text{-}Oc}$ denotes the transformation matrix; $L^{\times}{}_{Oc\text{-}i}$ is the antisymmetric vector moment of the segment i segment to the point O_c; α and β are the angle of attack and side-slip angle, $\alpha=\tan^{-1}(w/u)$,$\beta=\sin^{-1}(v/(u^2+v^2+w^2)^{1/2})$, and the subscripts c and p denote the wing parachute and the load, respectively; C_{BL} denotes the lift coefficient, C_{BD} denotes the drag coefficient, and C_{BY} denotes the side-slip coefficient, and $C_{M\delta}$, $C_{R\delta}$, $C_{N\delta}$ are all aerodynamic coefficients; defining the control quantities $\delta_e=\delta_R+\delta_L$ and $\delta a=\delta_R+\delta_L$, with δ_R and δ_L being the wing parachute right side downdraft and left side downdraft scores (corresponding to the two sides of the rudder deflections, respectively); V_c denotes the velocity of the wing parachute; and ω_c denotes the wing parachute's angular velocity, with $\omega_c=[q_c\ q_c\ r_c]^T$; M_{cI1} is a 3×1 matrix related to the angular velocity.

3.2. Dynamic Modeling of Loads

The wing parachute is subjected to forces and their moments including aerodynamic forces and their moments have aerodynamic forces F_{pA} and their moments M_{pA}, gravitational forces F_{pG}, inertial forces F_{pI} and their moments M_{pI}, engine thrusts F_{pth} and their moments M_{pth}, and connecting line pulls F_{pT} and their moments M_{pT}, so the wing parachute is subjected to forces and their moments equation of state is as follows:

$$\begin{aligned}E_{Fp}\dot{x}&=-\begin{pmatrix}F_{pA}+F_{pG}+F_{pT}+F_{pth}+\\m_pL_{cI1}+m_pL_{pI3}\end{pmatrix}\\E_{Mp}\dot{x}&=-\begin{pmatrix}M_{pA}+M_{pT}+F_{pth}+\\J_pT_{pc}^T\omega_{p1}+M_{pth}\end{pmatrix}\end{aligned} \tag{16}$$

where

$$E_{Fp}=m_p\left[I_3\ L_{pI1}\ L_{pI2}\ 0_{3\times 4}\right]^T \tag{17}$$

$$E_{Mp}=\left[0_{3\times 3}\quad J_pT^T{}_{pc}\quad J_p\Omega_{p1}\quad 0_{3\times 4}\right]^T \tag{18}$$

$$F_{pG}=m_pg\left[-\sin\theta_c\quad \cos\theta_c\sin\phi_c\quad \cos\theta_c\cos\phi_c\right] \tag{19}$$

$$F_{pA}=0.5\rho V^2{}_pS_pC_{Dp}T_{pc}\left[\mathrm{c}\alpha_p\mathrm{c}\beta_p\quad \mathrm{s}\beta_p\quad \mathrm{s}\alpha_p\mathrm{c}\beta_p\right]^T \tag{20}$$

$$M_{pA}=0.5\rho V^2{}_pS_pc_p\left[0\quad C_{mp}+k_{cp}C_{mqp}q_p\quad 0\right]^T \tag{21}$$

$$F_{pth}=T_{pc}\left[K_f\delta_{pte}\quad 0\quad 0\right]^T \tag{22}$$

$$M_{pth}=T_{pc}\left[0\quad 0\quad a_pK_f\delta_{pta}\right]^T \tag{23}$$

$$\Omega_{p1}=\begin{bmatrix}0&-\sin\theta_{pc}\\1&0\\0&\cos\theta_{pc}\end{bmatrix} \tag{24}$$

where, C_{Dp} is the drag coefficient; c_p is the projected length of the load in the X_p axis; C_{mp} and C_{mqp} are the aerodynamic

deflection coefficients of the load; K_f is the quantity related to the propeller diameter, $K_f=\rho D_p^4 C_T$, D_p is the diameter of the propeller, and C_T is the coefficient of tension; a_p is the length of 1/2 load; J_p is the matrix of the rotational moment of inertia of the load; and the defining control quantities $\delta_{pte}=N_R^2+N_L^2$ and $\delta a=N_R^2-N_L^2$, N_R and N_L are the rotational speeds of the left and right motors, respectively.

3.3. Dynamic Modeling of Parachute Systems

In the power parachute system, the tension of the connecting line on the load and the wing parachute exists as a pair of interacting forces, and the magnitude of the pulling moments of the connecting line on the wing parachute and the load exists in a positive relationship with the relative yaw angle ψ_{pc}, the yaw angular velocity r_{pc}, and the connecting line tension, so that the overall force of the power parachute and its moments can be expressed as follows:

$$E\dot{x} = -F \tag{25}$$

Where

$$E = \left[E^T{}_F \; E^T{}_M \left[0_{4\times 8} \; I_4 \right]^T \right]^T \tag{26}$$

$$F = \begin{bmatrix} F_1 \\ M_1 \\ \omega_{pc} \\ p_c + \left(q_c \sin\phi_c + r_c \cos\phi_c \right) \tan\theta_c \\ q_c \cos\phi_c - r_c \sin\phi_c \end{bmatrix} \tag{27}$$

$$E_F = E_{Fc} + E_{Fp} \tag{28}$$

$$E_M = K\left[E^T{}_{Mp} \quad E^T{}_{Mc} \right]^T + R_M E_{Fc} \tag{29}$$

$$F_1 = F_{cG} + F_{cAR} + F_{cAB} + F_{pA} + F_{pG} + F_{pth} + m_p\left(L_{cI1} + L_{pI3} \right) \tag{30}$$

$$M_1 = c_m \begin{bmatrix} M_{pA} + M_{pth} + J_p T^T{}_{pc} \dot{\omega}_{p1} \\ M_{cAR} + M_{cAB} + M_{cI1} \end{bmatrix} + \begin{bmatrix} 0_{4\times 1} \\ cr_{pc} \end{bmatrix} + R_M F_{c1} \tag{31}$$

$$R_m = \begin{bmatrix} -c_{m1}\left[L^T{}_{pT2} \quad L^T{}_{cT1} \right]^T T^T{}_{pc} \\ k\left[0 \quad 0 \quad 1 \right]^T \psi_{pc} \end{bmatrix}^T \tag{32}$$

$$F_{c1} = F_{cG} + F_{cAR} + F_{cAB} \tag{33}$$

At this point, the 8-degree-of-freedom model of the distributed power parachute has been established.

4. Characterisation of the Simulation

To validate the established model and assess the feasibility of the differential control mode, an 8 DOF differential control parafoil simulation system was constructed using MATLAB. The essential parameters of the wing parachute and payload necessary for modeling are presented in Table 1.

Utilizing the established system model, the motion characteristics of the parafoil system were analyzed. The simulation of these characteristics is based on the dynamic response of the parafoil system under various control inputs, including symmetric flap deflection control δ_{ce}, asymmetric flap deflection control δ_{ca}, symmetric thrust control δ_{pte}, and asymmetric thrust control δ_{pta}, as defined in Section III.

Table 1. Basic parameters of wing parachute

Parameters	Value	Unit
Span	15	m
Chord	5	m
Area of canopy	45	m2
Height of arc	2	m
Thicknesses	0.6	m
Aspect ratio	3	-
Rigging clamp angle	86	°
Length of lines	5	m
Mass of canopy	12	kg
Mass of payload	100	kg
Surface area of a payload	4.48	m2
Length of payloads	1	m
Width of the payload	0.8	m
Height of the payload	0.8	m

Initially, the impact of symmetric flap deflection control volume on the parafoil's motion characteristics was analyzed. The initial horizontal velocity of the wing parachute was set at 15 m/s (with no lateral or longitudinal velocity), and both the initial yaw and pitch angles were 0°.

At the 50th second, δ_{ce} =10°, δ_{ca} =0°, δ_{pte} =50N, δ_{pta} =0N. The simulation duration was 200 seconds. Figures 4, 5, and 6 illustrate the parafoil's three-axis velocity change curve, attitude angle change curve, and attitude angular velocity change curve, respectively. As illustrated in Figure 4, under the influence of symmetric flap deflection control volume, the system velocities along the x and z axes, u and w, decrease to some extent after a brief oscillation, while the y-axis velocity, v, remains largely unchanged. This is attributed to the increased drag caused by flap deflection, resulting in reduced speed; As depicted in Figure 5, following the application of the control volume, the system's yaw and roll angles exhibit no change, while the pitch angle experiences minor fluctuations after a brief oscillation; as shown in Figure 6, akin to the attitude angle, the attitude angular velocity exhibits only minor fluctuations in the pitch angle.

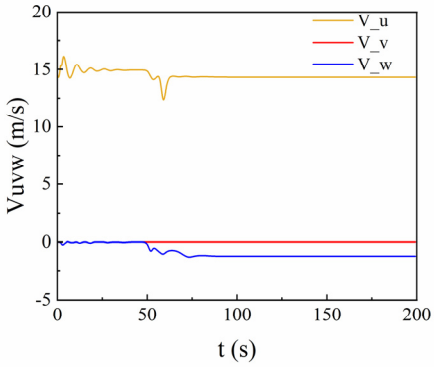

Fig 4. Parafoil 3-axis velocity variation curve

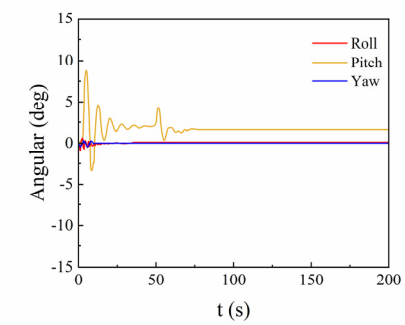

Fig 5. Parafoil Attitude Angle Variation Curve

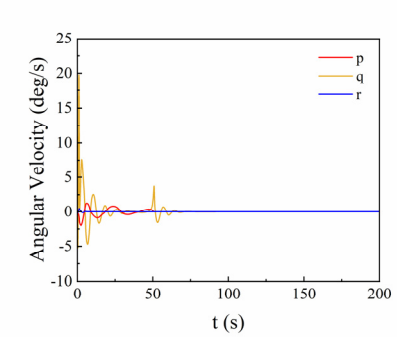

Fig 6. Parafoil Attitude Angular Velocity Variation Curve

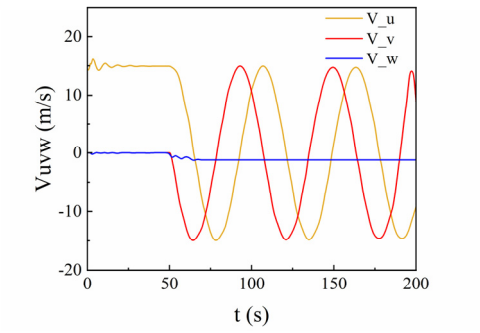

Fig 7. Parafoil 3-axis velocity variation curve

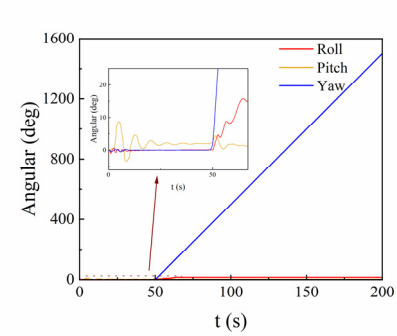

Fig 8. Parafoil Attitude Angle Variation Curve

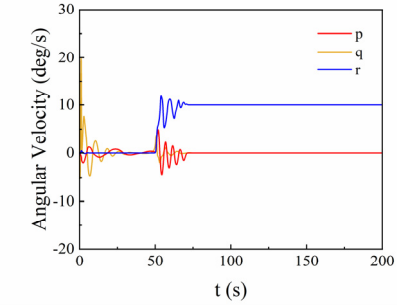

Fig 9. Parafoil Attitude Angular Velocity Variation Curve

The initial conditions of the simulation remained unchanged. To ensure experimental comparability, δ_{ca} =10° at the 50th second, while other control quantities remained unchanged. Figures 7, 8, and 9 display the three-axis velocity change curve, attitude angle change curve, and attitude angular velocity change curve of the parafoil, respectively. As illustrated in Figure 7, under the influence of asymmetric flap deflection control, the system velocities along the *x* and *y* axes, *u* and *v*, change periodically, while the *z*-axis velocity, *v*, decreases slightly after a brief oscillation. This is due to the yaw aerodynamic moment generated by asymmetric flap deflection, causing the wing parachute to exhibit yawing motion; As depicted in Figure 8, after applying the control quantity, the system's yaw angle increases steadily, the roll angle increases slightly after a brief oscillation, and the pitch angle remains essentially unchanged.

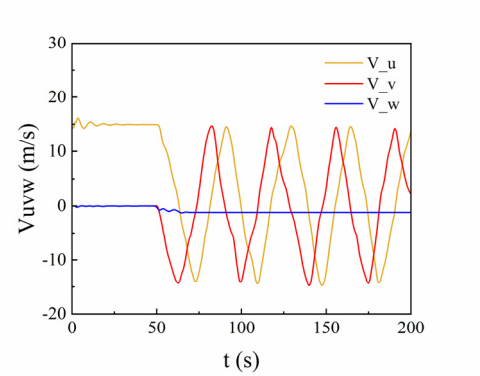

Fig 10. Parafoil 3-axis velocity variation curve

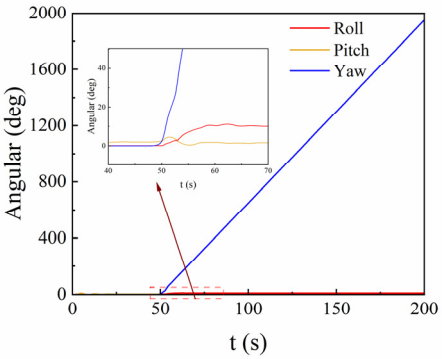

Fig 11. Parafoil Attitude Angle Variation Curve

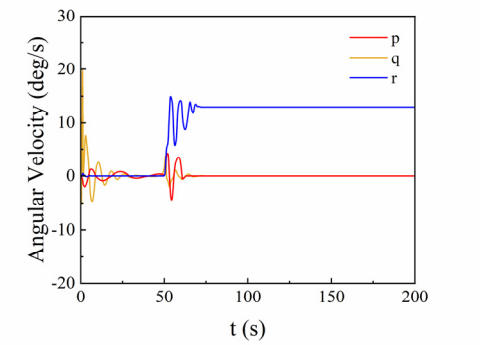

Fig 12. Parafoil Attitude Angular Velocity Variation Curve

The initial conditions of the simulation remained unchanged. At the 50th second, δ_{ca} =10°, δ_{pta} =10N are given, while other control quantities remained unchanged. Figures 10, 11, and 12 depict the parafoil's three-axis velocity change curve, attitude angle change curve, and attitude angular velocity change curve, respectively. As illustrated in Figure 10, under the combined influence of asymmetric flap deflection and asymmetric thrust control, the system velocities along the *x* and *y* axes, *u* and *v*, continue to change periodically, with an increased frequency. Meanwhile, the *z*-axis velocity, *v*, decreases slightly after a brief fluctuation. This is because the asymmetric flap deflection generates a yawing aerodynamic moment, causing the wing parachute to exhibit yawing motion. As depicted in Figure 11, following the application of the control quantity, the system's yaw angle increases steadily, the roll angle increases slightly after a brief oscillation, and the pitch angle remains essentially unchanged; as illustrated in Figure 12, the yaw angular velocity rapidly increases to 13 degrees per second, then stabilizes after a brief

oscillation, while the roll angular velocity remains unchanged at 0 following an oscillation. The aforementioned simulation phenomena indicate that the system's response speed to yaw control inputs increases significantly following the application of asymmetric thrust control.

This paper analyzes the relative pitch and yaw motions between the wing parachute and payload following the input of three control quantities. Figures 13 and 14 illustrate the relative pitch and yaw change curves, respectively. As illustrated in Figure 13, due to thrust influence, the parafoil system exhibits a small range of relative pitching motion, which remains within permissible limits. Following the input of control quantities, the relative pitch angle initially fluctuates briefly and then increases. However, compared to the previous two control inputs, the asymmetric flap yaw and asymmetric thrust inputs result in the smallest relative pitching motion. As depicted in Figure 14, the system itself exhibits no relative yaw motion. Following symmetric flap deflection, the relative yaw angle experiences minimal fluctuation, which is negligible. With asymmetric flap deflection and asymmetric thrust input, the relative yaw angle converges after fluctuating and is significantly reduced compared to that with asymmetric flap deflection.

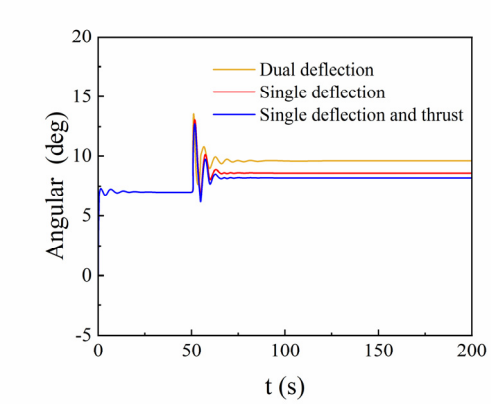

Fig 13. Relative Pitch Angle Change Curve

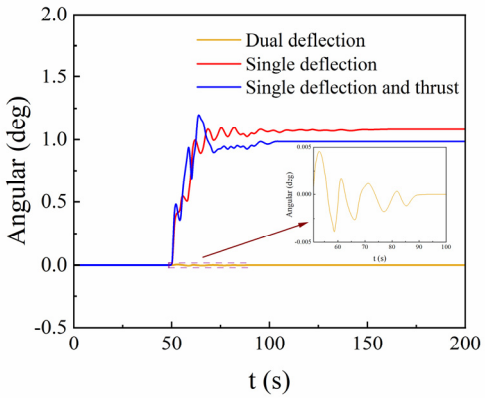

Fig 14. Relative yaw angle variation curve

In summary, the dynamic analysis of the parafoil system proves effective, with simulation results aligning consistently with experimental data from related literature. The established 8-DOF dynamic model accurately describes the flight state of the parafoil. Furthermore, it verifies that the proposed method of employing differential thrust and asymmetric flap deflection to enhance the response speed to yaw motion is feasible.

5. Conclusion

This paper presents the design of a distributed parafoil with a large load, developed against the backdrop of transportation. Initially, the payload and the forces and moments acting on the wing parachute are analyzed. Subsequently, the 8-DOF dynamic model of the distributed parafoil is derived through coordinate system transformation and elimination of internal forces and moments. Through simulation experiments, the motion characteristics are analyzed, and the model's validity is verified. This distributed parafoil exhibits a greater yaw motion response speed compared to traditional parafoils, and it improves the relative motion between the wing parachute and payload to some extent, thereby facilitating precise control of a large payload parafoil. Future research will focus on controller and trajectory tracking development based on this work, along with the construction of a parafoil experimental platform for testing.

Acknowledgments

This work is supported by the Scientific and Technological Research Program of Chongqing Municipal Education Commission (Grant No. KJZD-M202100702).

References

[1] Wang, H. Research on the Flight Controller of Unmanned Powered Parachute Vehicle [D]. Shenyang Aerospace University, 2021. DOI:10.27324/d.cnki.gshkc.2021.000119.

[2] Kong, L. Research on Autonomous Landing Visual Positioning System for Unmanned Powered Parachute Vehicle [D]. Shenyang Aerospace University, 2021. DOI:10.27324/d. cnki. gshkc. 2021.000049.

[3] Mihai, R., Pahonie, C. R., & Edu, I. A Practical Method to Estimate the Aerodynamic Coefficients of a Small-Scale Paramotor [J]. INCAS Bulletin, 2014, 6(4): 63-73. DOI:10. 13111/ 2066-8201.2014.6.4.6.

[4] Sun H ,Sun Q ,Wu W , et al.Altitude control for flexible wing unmanned aerial vehicle based on active disturbance rejection control and feedforward compensation[J].International Journal of Robust and Nonlinear Control,2020,30(1):222-245. DOI: 10.1002/rnc.4758.

[5] Luo S ,Sun Q ,Sun M , et al.On decoupling trajectory tracking control of unmanned powered parafoil using ADRC-based coupling analysis and dynamic feedforward compensation [J]. Nonlinear Dynamics,2018,92(4):1619-1635. DOI: 10.1007/ s11071-018-4150-0.

[6] Ochi Y, Watanabe M. Modelling and simulation of the dynamics of a powered paraglider[J]. Proceedings of the Institution of Mecanical Engineers Part G-Journal of Aerospace Engineering. 2011, 373-386. DOI: 10.1177/ 09544 100JAERO888.

[7] Qian, K., & Chen, Z. 8-DOF Dynamics Model and Simulation of a Powered Paraglider [J]. Command Control & Simulation, 2011, 33(01): 51-55. DOI:10.3969/j.issn.1673-3819.2011. 01. 013.

[8] Tao, J. Modeling and Homing Control Research of Wing Parachute System in Complex Environments [D]. Nankai University, 2017. Retrieved from http://www.cnki.net.

[9] Chen, S., Sun, Q., Chen, Z., et al. Longitudinal Cascade Control of Powered Parafoil Based on Speed Feedback [J]. Control Engineering of China, 2021, 28(01): 77-83. DOI:10.14107/ j.cnki. kzgc.20180289.

[10] Li Z ,Nan Y .Optimal Path Planning and Tracking Control Methods for Parafoil[J].Applied Sciences,2023,13(14): DOI: 10.3390/app13148115.

[11] Zhu E ,Sun Q ,Tan P , et al.Modeling of powered parafoil based on Kirchhoff motion equation[J].Nonlinear Dynamics, 2015, 79(1):617-629. DOI 10.1007/S11071-014-1690-9.

[12] Li, Y. Research on Dynamic Modeling and Autonomous Homing Technology of Wing Parachute System [D]. Nanjing University of Aeronautics and Astronautics, 2021. DOI:10. 27239/ d.cnki.gnhhu.2021.001227.

[13] Goodrick T F. Simulation studies of the flight dynamics of gliding parachute system[R]. AIAA:1979-0417. DOI:10. 2514/6. 1979-417.